Nanoscale

Accepted Manuscript

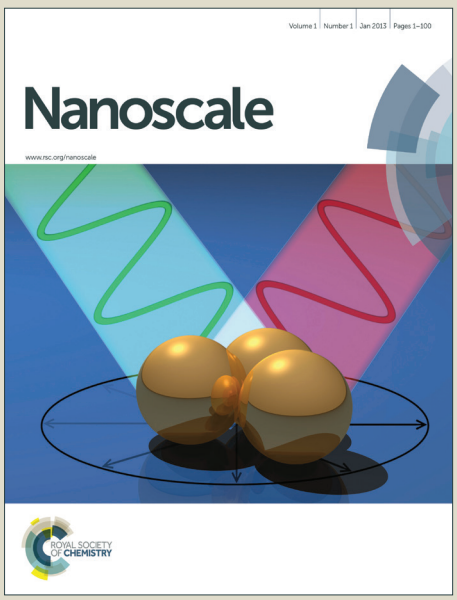

ROYAL SOCIETY OF CHEMISTRY

www.rsc.org/nanoscale

Biosafety Evaluations of Well-Dispersed Mesoporous Silica Nanoparticles: Towards in Vivo-Relevant Conditions

Tsang-Pai Liu[∥,†,§], *Si-Han Wu*[#,‡], *Yi-Ping Chen*[#,‡], *Chih-Ming Chou*[∥,⊥,*] *and Chien-Tsu Chen*[∥,⊥,*]

† Mackay Junior College of Medicine, Nursing and Management, Taipei, Taiwan; §Department of Surgery, Mackay Memorial Hospital, Taipei, Taiwan; #Department of Chemistry, National Taiwan University, Taipei, Taiwan; ‡ Research Center for Applied Sciences Academia Sinica, Taipei, Taiwan; ∥ Graduate Institute of Medical Sciences, College of Medicine, Taipei Medical University, Taipei, Taiwan; ⊥ Department of Biochemistry and Molecular Cell Biology , College of Medicine, Taipei Medical University, Taipei, Taiwan

E-mail: chenctsu@tmu.edu.tw; cmchou@tmu.edu.tw

KEYWORDS Mesoporous silica nanoparticles, surface modification, protein corona, zebrafish, nanotoxicology

ABSTRACT

This study aimed to investigate how mesoporous silica nanoparticles (MSN), especially focus on their surface functional groups, interacted with Raw 264.7 macrophages as well as with zebrafish embryos. Upon introducing nanoparticles into a biological milieu, adsorption of proteins and biomolecules onto nanoparticle surface usually progresses rapidly. Nanoparticles bound with proteins can result in physiological and pathological changes, but the mechanisms remain to be elucidated. In order to evaluate how protein corona affected MSN and the subsequent cellular immune responses, we experimented in both serum and serum-deprived conditions. Our findings indicated that the level of p-p38 was significantly elevated by the positively charged MSN, whereas negatively charged MSN resulted in marked ROS production. Most significantly, our experiments demonstrated the presence of protein efficiently mitigated the potential nano-hazard. On the other hand, strongly positively charged MSN caused 94% of the zebrafish embryos to die. In that case, the toxicity caused by the quaternary ammonium ligands on the surface of those nanoparticles was exerted in a dose-dependent manner. In summary, these fundamental studies here provide valuable insights to the design of better biocompatible nanomaterials in the future.

1. INTRODUCTION

As the fast development of state-of-art mesoporous silica nanoparticles (MSN) have been applied to *in vitro* and *in vivo* biological applications,[1-3] studies focusing on biocompatibility, safety and bioadhesive properties should be conducted to inform future clinical guidance. Recently, a comprehensive study highlights protein corona neutrality as an important design consideration, and demonstrated that even little difference in the surface heterogeneity (therein, i.e. spatial arrangement and relative exposure of surface amines) can result in profoundly different interactions with cells and tissues.[4] However, lack of knowledge about how the protein corona alters the cell response, particularly at the molecular level. Upon exposing nanoparticles to the physiological environment, the surface of nanoparticles is immediately decorated with the suspending proteins.[5, 6] Subsequently, what exactly the cells see now is the new assembly component called "biological identity", but not merely the nanoparticle "synthetic identity".[6, 7] Next, the biological identity will mediate their communication with cellular machinery followed by a serious complication of interactions and cell signaling pathways. It is noted that the biological identity and their evolution are governed by the dynamic nature of biological environments.[8, 9] The formation of protein corona surrounding the nanomaterials can induce dramatically physiological and pathological changes in cellular internalization pathway,[10, 11] immune response,[12] cytotoxicity,[13, 14] genotoxicity,[15] protein fibrillation[16] and targeting ability.[17] It is generally believed that the nanoparticle–corona complexes, instead of the bare nanomaterials, determine their *in vivo* biodistribution and biokinetics.[18] For example, binding of the apolipoprotein E to the surface of the polysorbate-coated nanoparticle enabled them to cross the blood brain barrier (BBB) *in vivo* and thus transported bound dalargin or loperamide into the brain[19]; nonspecific binding of proteins to nanoparticles may result in cell clearance by macrophages through the reticuloendothelial system (RES) of the liver and spleen.[18] In addition, the complex nano/bio/environment interactions, i.e. the properties of nanoparticles,[20, 21]cell types,[10] and culture media[22] could cause a noticeable impact on protein corona.

Therefore, in order to successfully predict the consequences of biological interactions between nanoparticles and the cells, experimental parameters should be carefully optimized for utilization of protein corona 'fingerprint' in nanomaterial design.[23]

To investigated the "intrinsic" properties of MSN, such as size[24], charge[25] and surface[26] interaction with cells, a lot of studies were conducted under serum-deprived conditions. One of the main reasons is to minimize the effects caused by the "extrinsic" properties derived from the environment (mainly the protein content); the other reason is to avoid the possible aggregation of nanoparticles by protein-mediated neutralization. However, because serum-free media cannot represent real *in vivo* exposure scenarios, recently there were several reports that attempted to minimize the interference of sera as well as to remain well dispersed in biological conditions by fabricating nanoparticles with PEG or zwitterions functionalization.[27, 28] Even more extremely, corona-free nanoparticles were synthesized and could be used to evaluate nanoparticle-cell behavior dictated directly by grafting ligands remained on the nanoparticle surface.[29] Furthermore, both theoretical models and several experimental reports have shown that the cellular uptake *via* endocytosis is size-dependent, and being of optimal efficiency when particles with diameters ranging between 30 to 60 nm.[30, 31]

In order to evaluate the potential nano-hazards and the relevant biodistribution, this study aimed to study how MSN interacted with Raw 264.7 macrophages *in vitro* and zebrafish *in vivo*. We prepared well-suspended MSN by PEGylation and subsequently decorated them with various surface modifications. Four types of MSN@PEG with diameter of 45 nm and different zeta potentials (from -52.0 mV to +38.9 mV) were chosen. Interactions between these nanoparticles and Raw 264.7 macrophages were studied both in serum-free as well as serum-containing media. We found the dramatic effects of the surface grafting on phospho-p38 expression and ROS production in these cells. In addition, we investigated cellular uptake of these nanoparticles and how that was associated with the expression of NF-κB p65 by confocal imaging, and the potential impacts on cell cycle progression by flow cytometry.

2. EXPERIMENTAL SECTION

2.1 Chemicals and Reagents

All reagents were used as received without further purification. *N*-Trimethoxysilylpropyl-*N*,*N*,*N*-trimethylammonium chloride (TMAC, 50% in methanol), (3-Trihydroxysilyl)propylmethylphosphonate (THPMP, 42% in water), and 2-(methoxy(polyethyleneoxy)propyl)trimethoxysilane (PEG-silane, molecular weight 460-590 g mol^{-1}, 90%) was purchased from Gelest. Cetyltrimethylammonium bromide (CTAB, 99+%), 3-aminopropyltrimethoxysilane (APTMS, 95%), ammonium hydroxide solution (28~30 wt% NH_3 in H2O) , fluorescein isothiocyanate isomer (FITC), and tetraethyl orthosilicate (TEOS, 98%) were purchased from Acrös. Rhodamine B isothiocyanate (RITC) were purchased from Sigma-Aldrich. Absolute ethanol was purchased from Shimakyu's Pure Chemicals. Ultrapure deionized (D.I.) water was generated by a Millipore Milli-Q plus system.

2.2 Synthesis of PEGylated Mesoporous Silica Nanoparticles with Various Surface Charges

PEGylated mesoporous silica nanoparticles (MSN@PEG) incorporated with red emitting rhodamine B dye (RITC) were synthesized by a method described in a previous study.[24, 32] After removal of surfactants, the obtained nanoparticles with weakly negative-charged surface are designated as wn-R-MSN@PEG. Separately, wn-R-MSN@PEG was further modified with THPMP-silane and TMAC-silane respectively by post-modification to obtain strongly negative (sn), strongly positive (sp), and weakly positive (wp)-charged R-MSN@PEG. For sn-R-MSN@PEG/THPMP synthesis, 100 mg of wn-R-MSN@PEG were first dispersed in a mixture of 40 mL of H_2O and 0.5 mL of NH_4OH. Next, 10 mL of 0.22 M aqueous THPMP solution was added with vigorous stirring at 40 °C for 4 h. For wp-R-MSN@PEG/TMAC and sp-R-MSN@PEG/TMAC synthesis, 100 mg of wn-R-MSN@PEG dispersed in 50 mL of EtOH were stirred under reflux for 4 h with 0.18 and 1.8 mmole TMAC-silane respectively. Products were collected by centrifuging at 11000 rpm for 60 minutes and washed by 95% ethanol for several times. Finally, the nanoparticles were kept in 99.5% ethanol. For some experiments, FITC-

labeled and non-fluorescent MSN were also prepared to avoid the interference from the color of fluorescence.

2.3 Cytotoxicity Assay

3×10^5 Raw 264.7 cells per well were seeded in 24-well plates for proliferation assays. After incubation with different amounts of nanoparticles suspension in serum-free DMEM or serum-containing DMEM for 4 h, the nanoparticles-treated cells were washed twice with culture medium followed by incubation with WST-1 reagent (Clontech) for 2 h at 37 °C for proliferation assay. Cell viability was determined by the formazan dyes generated by the live cells and the absorbance at 450 nm was measured using a microplate reader (Bio-Rad, model 680).

2.4 Western Blot Analysis

After each treatment, protein extracts (30 μg) were separated on a 10% SDS-PAGE, and the proteins were then electrophoretically transferred to a polyvinylidene difluoride (PVDF) membrane and blocked 1 h at room temperature in TBST buffer [1X Tris-buffered saline (TBS) containing 0.1% Tween 20] with 5% w/v nonfat dry milk. Membranes were incubated overnight at 4 °C with primary antibodies. p-p38 was diluted in TBST with 5% w/v BSA (1: 500 dilutions; Cell Signaling Technology), and α-tubulin was diluted in TBST with 5% w/v milk (1:15000 dilutions; Santa Cruz, CA). TVDF membranes were extensively washed and incubated with a horseradish peroxide-conjugated secondary immunoglobulin G antibody (1: 2000 dilution; Santa Cruz, CA) in blocking buffer for 1 h at room temperature. Immuno-reactive bands were visualized with the enhanced chemiluminescence substrate kit (Amersham Pharmacia Biotech, GE Healthcare UK Ltd, Bucks, UK) according to the manufacturer's protocol.

2.5 Superoxide Detection

The production of superoxide anion was fluorometrically estimated using a fluorescent probe, dihydroethidine (DHE), which is oxidized to a fluorescent intercalator, ethidium, by cellular oxidants, in particular, superoxide radicals. To measure superoxide anion generation, dihydroethidine (DHE; 5 μM) was used. Increase in DHE fluorescence upon paraquat (superoxide anion generator) stimulation

indicated an increase in superoxide anion levels. After various experimental treatments, fluorescence images were obtained with a fluorescence microscope (IX-71, Olympus) and quantitative data were analysis with flow cytometry.

2.6 Confocal Microscopic Examination

Nanoparticles-treated Raw 264.7 cells were fixed with 4% paraformaldehyde and permeabilized with 0.1% Triton X-100. After being washed in PBS, cells were blocked in blocking buffer [1xTris-buffered saline (TBS)-0.1% Tween 20, 5% w/v BSA] for 1 h and then incubated with a NF-κB p65 (1:50 dilution; Santa Cruz, CA) primary antibody in blocking buffer for 18 h at 4 °C. The cells were extensively washed and incubated with Alexa-568 fluorescein-labeled secondary antibody in blocking buffer at a dilution of 1/200 for 2 h, and counterstained for nuclei with 4',6-diamidino-2-phenylindole (DAPI; DNA marker) for 1 min. The fluorescent images were obtained with a confocal laser scanning microscope (TCS SP5, Leica).

2.7 Cell Cycle Analysis

Raw 264.7 cells were seeded at 2×10^6 cells per well in 6 cm dishes and allowed to attach for 24 h at 37 C. Then, the medium was removed and cells washed in serum-free medium. Raw 264.7 cells were incubated with 200 mg mL^{-1} of nanoparticles in serum-free medium for 4 h. Then, washed cells were exposed to 0.5 mM PQ in serum medium for 24 h. After washing and re-suspension, Raw 264.7 cells were analyzed by flow cytometry using propidium iodide (PI) staining. Statistical analyses were performed using ModFit LT software (Verity Software House, Topsham, ME).

2.8 Zebrafish Maintenance

Zebrafish (*Danio rerio*) were obtained from zebrafish core facility of Taipei Medical University and maintained at 28 °C on a 14 h light/10h dark cycle. All animal procedures were approved by Taipei Medical University Institutional Animal Care and Utilization Committee (TMU-IACUC). Embryos were incubated at 28 °C and different developmental stages were determined according to the Zebrafish Book.[33]

2.9 Zebrafish Toxicity Test

The wild-type embryos were exposed to nanoparticles (50 or 100 ug mL^{-1}) at 20 hpf for 5-144 h to evaluate toxic effects on zebrafish embryos. Eight dechorionated embryos were treated with 2 mL (50 or 100 μg mL^{-1}) of nanoparticles in one well of 24-well chamber. After exposed to nanoparticles for 5 h and 96 h (4 dpf), the percentage of fish survival rate was shown. During the exposure period, the photographs of embryos malformation were observed under an Olympus IX70-FLA inverted fluorescence microscope (Olympus, Tokyo, Japan). Images were taken by using the SPOT digital camera system (Diagnostic Instruments, Sterling Heights, Michigan, USA) and assembled by ImageJ program.[34]

2.10 Characterization

Transmission electron microscopy (TEM) images were taken on a JEOL JSM-1200 EX II operating at 100 kV. Size measurements were performed using dynamic light scattering (DLS) on a Malvern Zetasizer Nano ZS (Malvern, UK). Zeta potential was determined by the electrophoretic mobility and then applying the Henry equation on Malvern Zetasizer Nano ZS (Malvern, UK). Fluorescent images were obtained on a confocal microscope (TCS SP5, Leica). An elemental analyzer (Elementar vario EL cube, Thermal Conductivity Detector) was used to determine the precise nitrogen content in the composite. Thermogravimetric analysis (Mettler Toledo TGA/DSC1) was carried out with a heating rate of 10 °C min^{-1} from 100 to 800 °C with an Ar flow-rate of 50 mL min^{-1}.

3. RESULTS

3.1 Characterization of Functionalized Mesoporous Silica Nanoparticles

Well-suspended, uniform, and RITC-incorporated MSNs (designated as R-MSN), with an average diameter of 45 nm according to TEM (Figure 1a and Figure S1a-b), were prepared under dilute tetraethyl orthosilicate (TEOS) and low surfactant (CTAB) conditions *via* an ammonia-catalyzed sol-gel process.[24, 32] To avoid irreversible aggregation, which often occurs during the surfactant removal process and centrifugation, the poly(ethylen glycol) (PEG-silane) was further introduced on the surface of the as-synthesized bare MSN before the surfactant removal step. PEGylation has been shown to increase the

dispersity and stability of nanoparticles, especially in the biological milieu, to prolong blood circulation *in vivo* through its hydrophilicity and steric repulsion effects,[18, 27] and to reduce the hemolytic activity.[32, 35] After removal of surfactants, the weight percentage of PEG units in the wn-R-MSN@PEG (wn stands for weakly negative-charged) was estimated to be about 12% based on thermogravimetric analysis (TGA, Figure S1c). To obtain representative surface charge of MSN, the wn-R-MSN@PEG was further modified with negatively charged THPMP-silane in a basic aqueous solution and with positively charged TMAC-silane in ethanol, respectively. Finally, four types of R-MSN@PEG with various zeta potentials were obtained: wn-R-MSN@PEG (weakly negative-charged), sn-R-MSN@PEG/THPMP (strongly negative-charged), wp-R-MSN@PEG/TMAC (weakly positive-charged), and sp-R-MSN@PEG/TMAC (strongly positive-charged). Quantitative analyses of these nanoparticles were carried out based on the percentage weight loss in the TGA curve (Figure S1c). Moreover, as shown in Figure 1b, the zeta potentials of the R-MSN@PEG derivatives were in the range from -52.0 to +38.9 mV, confirming the presence of the functional groups. For applications of nanoparticles in biological systems, dynamic light scattering (DLS) measurement has been used to investigate whether nanoparticles were discrete or aggregated in a given solution. Figure 1c shows that these four samples were thoroughly dispersed in H_2O, and their Z-average hydrodynamic diameters were below 60 nm, except for sn-R-MSN@PEG/THPMP. This is probably in part due to the stronger hydration of methylphosphonate. The stability of these samples was also evaluated by suspending them in cell culture media containing 10% fetal bovine serum (pH 7.4). It is noted that the additional peak at 10 nm and shoulder peak at ~50 nm of the hydrodynamic diameters are attributed to the serum proteins in the media (Figure 1d). As a result, comparing the hydrodynamic distribution of these nanoparticles measured in serum-free media (data not shown), slight broadening profiles of that were obtained in serum-containing media. Most importantly, no significant increase of the sample sizes was observed in culture media compared to that measured in H_2O, demonstrating their excellent colloidal stability under physiological conditions.

3.2 Effects of Functionalized Mesoporous Silica Nanoparticles on Cellular Uptake, Cytotoxicity

Adsorption of proteins onto the nanoparticle's surface forms a swaddling layer, known as the protein "corona", which usually induces changes in the physicochemical characteristics and the biological fate of nanoparticles, such as cellular internalization pathway and immune response.[36] To understand corona-affected cellular events, uptake studies were performed both in serum-containing and serum-free media. Firstly, to investigate the surface effect of nanoparticles on cell labeling, the uptake of various types of R-MSN@PEG by Raw 264.7 macrophages was examined by flow cytometry. As shown in Figure S2, Raw 264.7 cells were labeled with 200 μg mL^{-1} of various types of R-MSN@PEG for 4 h in both serum-free and serum-containing media. Next, to evaluate the *in vitro* cytotoxicity of various types of R-MSN@PEG, cell viability was examined by WST-1 assay. As shown in Figure S3, no significant change on cell proliferation was observed by the treatments of nanoparticles either for 4 h, or for 4 h followed by an additional 24 h of culture. No obvious effect on the cellular mitochondrial function caused by the nanoparticles was found at the indicated time points, regardless of the presence or absence of serum in the medium. In addition, Western blot was used to evaluate the expression of phospho-p38 (p-p38) in Raw 264.7 cells after nanoparticle treatments. Phospho-p38 is involved in inflammatory responses and reactive oxygen species-related diseases. As shown in Figure 2a, under serum-free media, MSN@PEG treatments affected the expression of p-p38 in a time-dependent pattern. Compared to the expression of p-p38 in the control cells, marked induction of p-p38 could be immediately detected after 4 h treatments with wn-MSN@PEG, wp-MSN@PEG/TMAC and sp-MSN@PEG/TMAC. However, when the cells were subsequently kept under a conventional culture condition for another 24 h, the expression of p-p38 in the sera with wn-MSN@PEG was almost disappeared, and was largely reduced in the experimental sets with positively charged wp-MSN@PEG/TMAC and with sp-MSN@PEG/TMAC. To compare the two positively charged nanoparticles, the more positively charged sp-MSN@PEG/TMAC induced a higher level of p-p38 in Raw 264.7 cells. For delivery of nanoparticles in serum-containing media, as shown in Figure 2b, similar effects on p-p38 caused by nanoparticles were observed, but the expression levels of p-p38 were

significantly lower. The expressions of p-p38 were about the same in the control and in the nanoparticle-treated cells after additional 1 day of culture in serum-containing media. In addition, sp-MSN@PEG/TMAC induced expression of p-p38 in a dose-dependent manner (100, 200 and 500 μg mL^{-1}) after 4 h of treatments, as evident in Figure S4. Again, lower expression of p-p38 was observed with sp-MSN@PEG/TMAC delivery in serum-containing media compared with that in serum-free media. As many cytotoxic effects of nanoparticles are usually associated with oxidative stress, we also evaluated the ability of various types of MSN@PEG to produce ROS in Raw 264.7 cells. As shown in Figure 2c, after separate treatments with each type of MSN@PEG on Raw 264.7 cells in serum-free media, a significant increase in ROS was found, suggesting oxidative stress was generated in each condition. Nevertheless, as shown in Figure 2d, there was no significant production of ROS when treated with either wn-MSN@PEG/THPMP or positively charged MSN@PEG/TMAC. But there was little increase of ROS in the treatment with sn-MSN@PEG/THPMP. We also used confocal images to verify the uptake of the most positively as well as the most negatively charged F-MSN@PEG by Raw 264.7 cells. As shown in Figure 3 and Figure S5, both sn-F-MSN@PEG/THPMP and sp-F-MSN@PEG/TMAC were readily engulfed by Raw 264.7 cells in 4 h either under serum or serum-deprived conditions. Immunofluorescence staining revealed similar levels of NF-κB p65, a master transcriptional regulator of pro-inflammation, expressed in nanoparticles-treated and paraquat (PQ, as the positive control)-treated Raw 264.7 cells. Compared to the relatively uniform distribution of NF-κB p65 in the PQ-treated Raw 264.7 cells, not all NF-κB p65 was translocated into the nucleus, but some NF-κB p65 still remained in the cytosol when cells were treated with nanoparticles under serum-containing conditions (as indicated by the white arrows in Figure 3). In addition, the degree of NF-κB translocation from the cytoplasm to the nucleus was obviously higher in the absence than the presence of serum when nanoparticles were delivered into Raw 264.7 cells (Figure 3 and Figure S5).

3.3 Cell Cycle Analysis by Flow Cytometry

The cell cycle progression of Raw 264.7 cells was evaluated with propidium iodide staining and quantified by flow cytometry (Figure 4). To evaluate whether the silica nanoparticles were involved in

eliciting cell cycle arrest, we analyzed cell cycles in Raw 264.7 cells in serum-containing media after treatments with various types of MSN@PEG at a dose of 200 μg mL^{-1} for 4 h. Our results clearly revealed that all four types of silica nanoparticles did not inhibit of the cell cycle progression from G0/G1 to S+G2/M phases.

3.4 Effects of Functionalized Mesoporous Silica Nanoparticles on the Mortality and Distribution of Zebrafish Embryos

To assess the potential toxicity of the various types of R-MSN@PEG at the organism level, zebrafish, a versatile *in vivo* vertebrate model for many areas of biologic investigation, was selected for this study. First, zebrafish embryos at 20 hpf were exposed to the four types of R-MSN@PEG at concentrations of 50 and 100 μg mL^{-1} for 5-144 hpf to test if nanoparticle treatments could be associated with mortality or developmental malformations. Table S1 showed the mortality of the zebrafish embryos that were exposed to different types of R-MSN@PEG at different concentrations and for different lengths of time. At the lower concentration of nanoparticles (50 μg mL^{-1}), no differences on the embryonic mortality were observed at 25 hpf between control and all the treatment groups (Figure 5a-5e). Very high embryonic mortality rates, up to 94% (15/16 deaths), was observed after exposure to sp-R-MSN@PEG/TMAC at the concentration of 100 μg mL^{-1} (Figure 5f) and sp-R-MSN@PEG/TMAC treated of epidermis disruption suspended cells (Figure 5g). Prolonged exposure (till to 144 hpf) did not result in more death of the zebrafish. As shown in Figure 5h, exposure of zebrafish embryos to positively charged R-MSN@PEG/TMAC, including the one survivor to sp-R-MSN@PEG/TMAC, resulted in obvious red fluorescence in the yolk, tail and sometimes in intestines. On the contrary, as shown in Figure 5i, strongly negative charged sn-R-MSN@PEG/THPMP was predominantly localized in the intestine, with no distinguishable fluorescence in the yolk or the tail at 4 dpf.

4. DISCUSSIONS

This study demonstrated that cellular uptake of these nanoparticles was efficient both in serum-containing and serum-free media according to our flow cytometry and confocal microscopy experiments.

Even though no significant changes in cell cycle progression and metabolic activity were observed, Western blot analysis and Reactive Oxygen Species (ROS) assays showed significant but different results; the p-p38 proteins were markedly increased particularly after the treatment with positive charged sp-R-MSN@PEG/TMAC, however, the ROS levels were distinctly increased by the treatment of negative charged R-MSN@PEG/THPMP. The translocation of NF-κB from the cytoplasm to the nucleus is usually regarded as a hallmark of its activation.[37] From the expressions of NF-κB p65 both in serum and serum deprivation conditions with the treatments of nanoparticles and paraquat, the predominantly cytoplasmic distribution of NF-κB p65 observed in some cells indicates the delayed or less activation of NF-κB p65. Considering the culture conditions and post-treatments, it is found that both the serum and additional culture period can mitigate the damage/response of cells caused by nanoparticles. In serum-free media (i.e. the absence of protein), a strong adhesion of the bare silica on the cell membrane and acquirement of corona from biomolecules in the cell membrane are indicative of cell damage.[11] Nevertheless, in serum-containing media, the preformed protein corona around nanoparticles could limit direct contact between nanoparticles and the cell membranes and thereby reduce acute cellular toxicity.[38] Our findings are in line with previous study results that show protein corona could reduce the damage imposed by nanoparticles,[39] and retain during nanoparticles uptake prior to nanoparticle degradation in the lysosomes.[40] Although the external protein corona (i.e. extrinsic component of nanoparticles) is where such molecular interaction takes place, the intrinsic components of nanoparticles (e.g. surface ligands) also play an important role in regulating certain signaling processes inside the cells such as cell cycle progression.[41, 42] Taken together, either bare nanoparticles or corona surrounding nanoparticles could engage with a wide range of biomolecules and subsequently impact the cellular responses.[43] Accordingly, nanoparticle delivery and absorbance in serum-containing media is a physiologically relevant event, which involves cell signaling pathways and could subsequently modify inflammation and immune responses.

Last but not least, we also used four types of R-MSN@PEG functionalized with various charges, and tested the biological responses in dechorionated embryonic zebrafish. We did not observe

nanoparticle-induced lethality in embryonic zebrafish, except during the exposure of sp-R-MSN@PEG/TMAC at the higher concentration (100 μg mL^{-1}). The very high embryo lethality (94 %) observed in the exposure of sp-R-MSN@PEG/TMAC might reflect the preferential uptake of sp-R-MSN@PEG/TMAC by the organism.[44] Our study results are very similar to the previous study,[45] in which the structure of quaternary ammonium used to make positively charged gold nanoparticles is exactly the same as the ligand on the surface of sp-R-MSN@PEG/TMAC. The unique surface structure of sp-R-MSN@PEG/TMAC might be related to their easy uptake and disrupted epidermis structure of the embryos, caused the cells release from embryo and subsequent lethality to the organism. In the future, more comprehensive studies of disrupted epidermis cell-cell junction molecular mechanism need to be investigated. On the other hand, no lethality was observed in embryos treated with either wp-R-MSN@PEG/TMAC or a lower dose of sp-R-MSN@PEG/TMAC. Notably, the number of TMAC on the surface of sp-R-MSN@PEG/TMAC (0.8 mmole of groups per gram of nanoparticles) is about five times that of wp-R-MSN@PEG/TMAC by element analysis. These results give important hints that the potential nano-hazards can be controlled using TMAC in a dose-dependent manner on the testing organism such as embryonic zebrafish. Though delivery of MSN into zebrafish *via* microinjection was reported previously,[46-48] to the best of our knowledge, this is the first report showing that the sn-R-MSN@PEG/THPMP could passively translocate from the solutions into embryos intestine region and stay inside the embryos throughout the embryonic development (144 hpf). It is possible that in the future, utilization of the surface modifications on R-MSN/PEG, one could possibly predict the biodistribution of these nanoparticles in a testing organism such as zebrafish here.

5. CONCLUSIONS

In summary, we have demonstrated that nanoparticles with various functional groups, including PEG, methylphosphonate, and quaternary ammonium groups, could be engineered to adjust the surface charges and dispersity property of the MSN. Consistent with previous findings,[13, 14, 49] we found that nanoparticle delivery in the presence of proteins could significantly reduce cellular inflammatory

responses. We investigated how *in vitro* cellular uptake, proliferation, oxidative stress, inflammatory responses, as well as cell cycle progression, were influenced by the nanoparticle surface interaction with Raw 264.7 macrophage cells. The formation of protein corona could activate unwanted phagocytosis and subsequently induce rapid clearance of nanoparticles from circulation. More significantly, the most challenging work might be the way to control and utilize the *in situ* forming protein corona instead of the chemical grafting on the nanoparticles to achieve targeting *in viv*o in future.[17] The doses of nanoparticles as well as the ability of the embryos to uptake certain nanoparticles could be the reasons resulting in the differential biological response, including the mortality and the biodistribution. More in-depth and complete understanding of the relationships linking the surface chemistry, hydrodynamic size, shape and composition of a nanomaterial to protein adsorption and phagocytic cell uptake are urgent. Future efforts should be devoted to minimizing potential nano-hazards and enabling more informative design of the next generation nanomaterials.[31, 50]

ASSOCIATED CONTENT

Supporting Information. TEM image, size distribution histogram of as-synthesized wn-R-MSN@PEG. TGA measurments. Cellular uptake efficiency. WST-1 analysis. Western blot assays. Confocal images and zebrafish mortality.

AUTHOR INFORMATION

Corresponding Author

chenctsu@tmu.edu.tw; cmchou@tmu.edu.tw

ACKNOWLEDGMENT The authors thank Ms. Ching-Wei Lu for her assistance with element analysis at the Department of Chemistry in National Taiwan University. The authors also thank Mr. Zih-An Chen for TGA measurements of this work.

REFERENCES

1. Y. Chen, H. Chen and J. Shi, *Adv. Mater.*, 2013, **25**, 3144-3176.
2. V. Mamaeva, C. Sahlgren and M. Linden, *Adv. Drug Delivery Rev.*, 2013, **65**, 689-702.
3. S. H. Wu, C. Y. Mou and H. P. Lin, *Chem. Soc. Rev.*, 2013, **42**, 3862-3875.
4. J. L. Townson, Y. S. Lin, J. O. Agola, E. C. Carnes, H. S. Leong, J. D. Lewis, C. L. Haynes and C. J. Brinker, *J. Am. Chem. Soc.*, 2013, **135**, 16030-16033.
5. P. d. Pino, B. Pelaz, Q. Zhang, P. Maffre, G. U. Nienhaus and W. J. Parak, *Mater. Horiz.*, 2014, **1**, 301-313.
6. M. P. Monopoli, C. Aberg, A. Salvati and K. A. Dawson, *Nat. Nanotechnol.*, 2012, **7**, 779-786.
7. C. D. Walkey and W. C. Chan, *Chemical Society reviews*, 2012, **41**, 2780-2799.
8. A. Albanese, C. D. Walkey, J. B. Olsen, H. Guo, A. Emili and W. C. Chan, *Acs Nano*, 2014, **8**, 5515-5526.
9. M. Lundqvist, J. Stigler, T. Cedervall, T. Berggard, M. B. Flanagan, I. Lynch, G. Elia and K. Dawson, *Acs Nano*, 2011, **5**, 7503-7509.
10. Y. Yan, K. T. Gause, M. M. Kamphuis, C. S. Ang, N. M. O'Brien-Simpson, J. C. Lenzo, E. C. Reynolds, E. C. Nice and F. Caruso, *Acs Nano*, 2013, **7**, 10960-10970.
11. A. Lesniak, F. Fenaroli, M. P. Monopoli, C. Aberg, K. A. Dawson and A. Salvati, *Acs Nano*, 2012, **6**, 5845-5857.
12. Z. J. Deng, M. Liang, M. Monteiro, I. Toth and R. F. Minchin, *Nat. Nanotechnol.*, 2011, **6**, 39-44.
13. W. Hu, C. Peng, M. Lv, X. Li, Y. Zhang, N. Chen, C. Fan and Q. Huang, *Acs Nano*, 2011, **5**, 3693-3700.
14. J. C. Kah, C. Grabinski, E. Untener, C. Garrett, J. Chen, D. Zhu, S. M. Hussain and K. Hamad-Schifferli, *Acs Nano*, 2014, **8**, 4608-4620.

15. L. Gonzalez, M. Lukamowicz-Rajska, L. C. Thomassen, C. E. Kirschhock, L. Leyns, D. Lison, J. A. Martens, A. Elhajouji and M. Kirsch-Volders, *Nanotoxicology*, 2014, **8**, 876-884.

16. M. Mahmoudi, H. R. Kalhor, S. Laurent and I. Lynch, *Nanoscale*, 2013, **5**, 2570-2588.

17. A. Salvati, A. S. Pitek, M. P. Monopoli, K. Prapainop, F. B. Bombelli, D. R. Hristov, P. M. Kelly, C. Aberg, E. Mahon and K. A. Dawson, *Nat. Nanotechnol.*, 2013, **8**, 137-143.

18. P. Aggarwal, J. B. Hall, C. B. McLeland, M. A. Dobrovolskaia and S. E. McNeil, *Adv. Drug Delivery Rev.*, 2009, **61**, 428-437.

19. J. Kreuter, D. Shamenkov, V. Petrov, P. Ramge, K. Cychutek, C. Koch-Brandt and R. Alyautdin, *J. Drug Target.*, 2002, **10**, 317-325.

20. M. P. Monopoli, D. Walczyk, A. Campbell, G. Elia, I. Lynch, F. B. Bombelli and K. A. Dawson, *J. Am. Chem. Soc.*, 2011, **133**, 2525-2534.

21. C. D. Walkey, J. B. Olsen, H. Guo, A. Emili and W. C. Chan, *J. Am. Chem. Soc.*, 2012, **134**, 2139-2147.

22. G. Maiorano, S. Sabella, B. Sorce, V. Brunetti, M. A. Malvindi, R. Cingolani and P. P. Pompa, *Acs Nano*, 2010, **4**, 7481-7491.

23. C. D. Walkey, J. B. Olsen, F. Song, R. Liu, H. Guo, D. W. Olsen, Y. Cohen, A. Emili and W. C. Chan, *Acs Nano*, 2014, **8**, 2439-2455.

24. F. Lu, S. H. Wu, Y. Hung and C. Y. Mou, *Small*, 2009, **5**, 1408-1413.

25. T. H. Chung, S. H. Wu, M. Yao, C. W. Lu, Y. S. Lin, Y. Hung, C. Y. Mou, Y. C. Chen and D. M. Huang, *Biomaterials*, 2007, **28**, 2959-2966.

26. Slowing, II, C. W. Wu, J. L. Vivero-Escoto and V. S. Lin, *Small*, 2009, **5**, 57-62.

27. S. Lowe, N. M. O'Brien-Simpson and L. A. Connal, *Polymer Chemistry*, 2015.

28. K. Pombo Garcia, K. Zarschler, L. Barbaro, J. A. Barreto, W. O'Malley, L. Spiccia, H. Stephan and B. Graham, *Small*, 2014, **10**, 2516-2529.

29. D. F. Moyano, K. Saha, G. Prakash, B. Yan, H. Kong, M. Yazdani and V. M. Rotello, *Acs Nano*, 2014, **8**, 6748-6755.

30. I. Canton and G. Battaglia, *Chem. Soc. Rev.*, 2012, **41**, 2718-2739.

31. A. Albanese, P. S. Tang and W. C. W. Chan, *Annu. Rev. Biomed. Eng.*, 2012, **14**, 1-16.

32. Y. S. Lin, N. Abadeer, K. R. Hurley and C. L. Haynes, *J. Am. Chem. Soc.*, 2011, **133**, 20444-20457.

33. M. Westerfield, *(2007)*, The zebrafish book. A guide for the laboratory use of zebrafish (Danio rerio), 5th edition. Eugene: University of Oregon Press.

34. C. A. Schneider, W. S. Rasband and K. W. Eliceiri, *Nat. Methods*, 2012, **9**, 671-675.

35. S. H. Wu, C. Y. Lin, Y. Hung, W. Chen, C. Chang and C. Y. Mou, *J. Biomed. Mater. Res. Part B*, 2011, **99**, 81-88.

36. C. D. Walkey and W. C. Chan, *Chem. Soc. Rev.*, 2012, **41**, 2780-2799.

37. P. A. Baeuerle and T. Henkel, *Annu. Rev. Immunol.*, 1994, **12**, 141-179.

38. L. Wang, J. Li, J. Pan, X. Jiang, Y. Ji, Y. Li, Y. Qu, Y. Zhao, X. Wu and C. Chen, *J. Am. Chem. Soc.*, 2013, **135**, 17359-17368.

39. J. A. Kim, A. Salvati, C. Aberg and K. A. Dawson, *Nanoscale*, 2014, **6**, 14180-14184.

40. F. Wang, L. Yu, M. P. Monopoli, P. Sandin, E. Mahon, A. Salvati and K. A. Dawson, *Nanomedicine : nanotechnology, biology, and medicine*, 2013, **9**, 1159-1168.

41. J. A. Kim, C. Aberg, G. de Carcer, M. Malumbres, A. Salvati and K. A. Dawson, *Acs Nano*, 2013, **7**, 7483-7494.

42. A. Lankoff, M. Arabski, A. Wegierek-Ciuk, M. Kruszewski, H. Lisowska, A. Banasik-Nowak, K. Rozga-Wijas, M. Wojewodzka and S. Slomkowski, *Nanotoxicology*, 2013, **7**, 235-250.

43. F. Marano, S. Hussain, F. Rodrigues-Lima, A. Baeza-Squiban and S. Boland, *Arch. Toxicol.*, 2011, **85**, 733-741.

44. S. L. Harper, J. L. Carriere, J. M. Miller, J. E. Hutchison, B. L. Maddux and R. L. Tanguay, *Acs Nano*, 2011, **5**, 4688-4697.

45. L. Truong, S. C. Tilton, T. Zaikova, E. Richman, K. M. Waters, J. E. Hutchison and R. L. Tanguay, *Nanotoxicology*, 2013, **7**, 192-201.

46. H. Yan, C. Teh, S. Sreejith, L. Zhu, A. Kwok, W. Fang, X. Ma, K. T. Nguyen, V. Korzh and Y. Zhao, *Angew. Chem. Int. Ed.*, 2012, **51**, 8373-8377.

47. F. Sharif, F. Porta, A. H. Meijer, A. Kros and M. K. Richardson, *Int. J. Nanomed.*, 2012, **7**, 1875-1890.

48. X. Ma, C. Teh, Q. Zhang, P. Borah, C. Choong, V. Korzh and Y. Zhao, *Antioxid Redox Signal*, 2014, **21**, 707-722.

49. S. Tenzer, D. Docter, J. Kuharev, A. Musyanovych, V. Fetz, R. Hecht, F. Schlenk, D. Fischer, K. Kiouptsi, C. Reinhardt, K. Landfester, H. Schild, M. Maskos, S. K. Knauer and R. H. Stauber, *Nat. Nanotechnol.*, 2013, **8**, 772-U1000.

50. S. T. Kim, K. Saha, C. Kim and V. M. Rotello, *Acc. Chem. Res.*, 2013, **46**, 681-691.

SYNOPSIS TOC

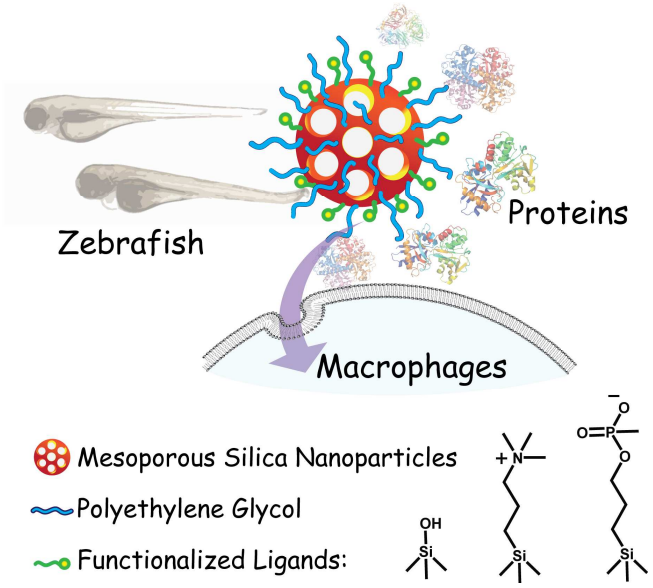

Figure 1

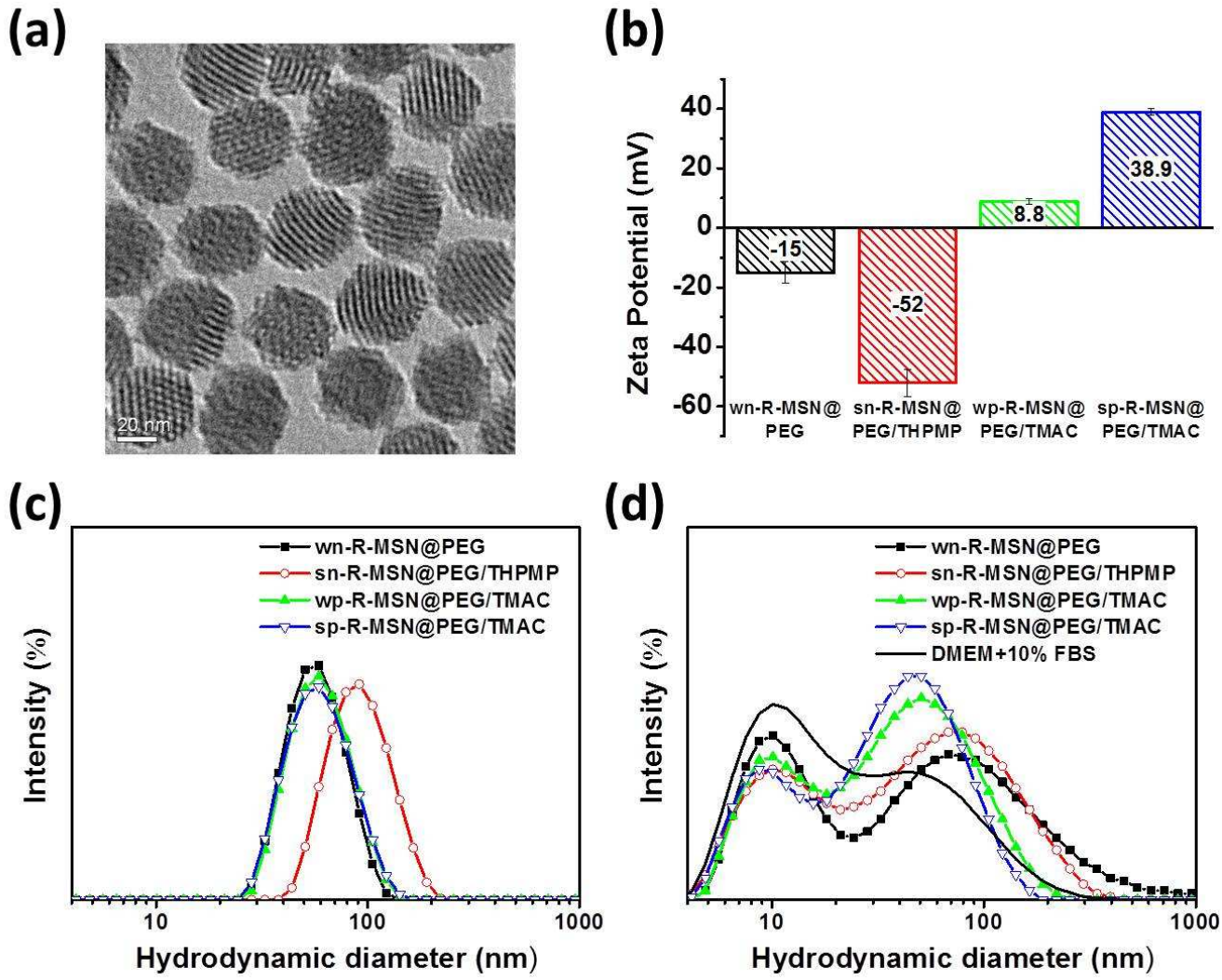

Figure 1. (a) TEM image of as-synthesized wn-R-MSN@PEG; (b) zeta potentials of various types of R-MSN@PEG; hydrodynamic diameter distributions of various types of R-MSN@PEG in (c) H_2O and (d) DMEM with 10% FBS.

Figure 2

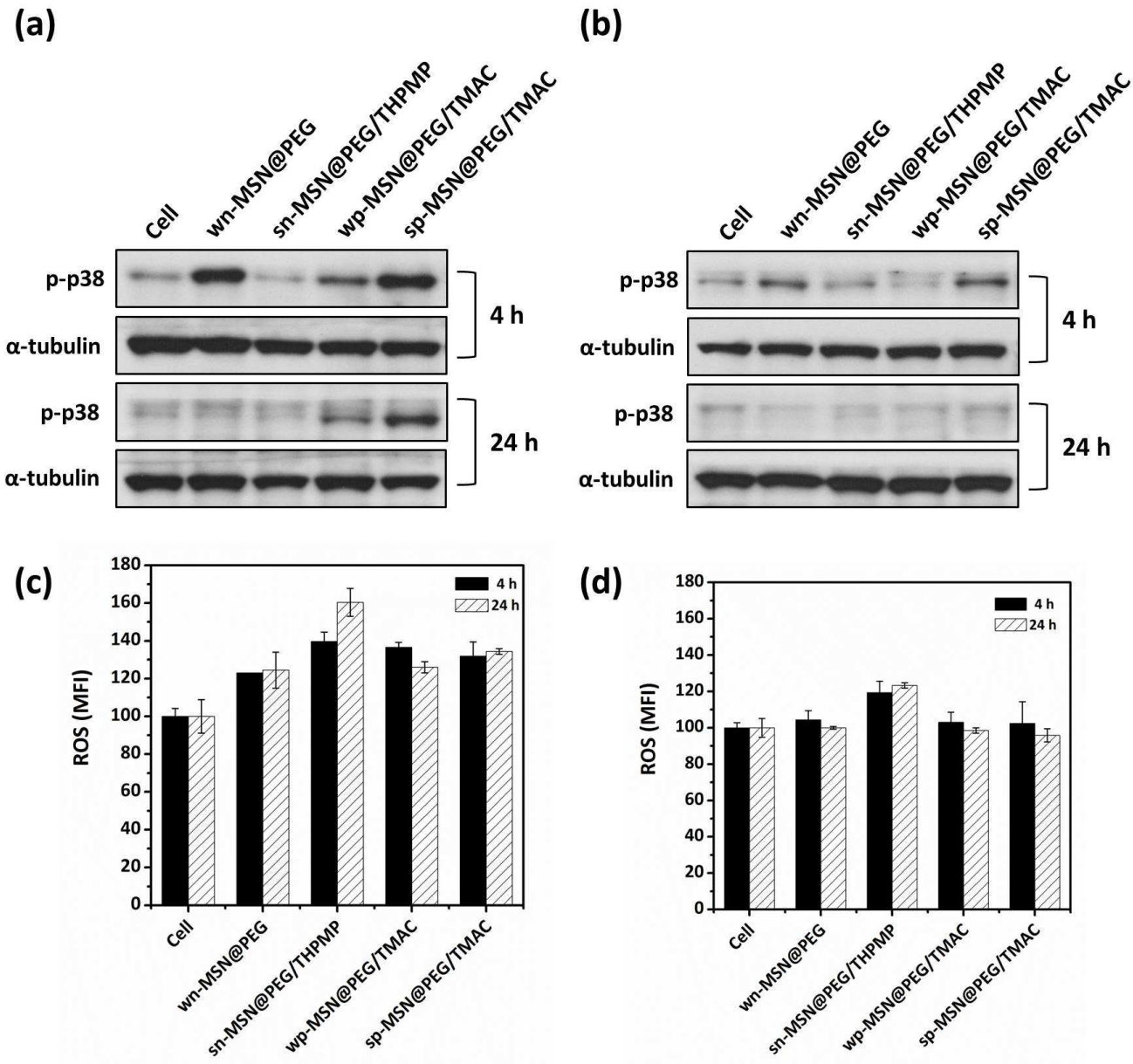

Figure 2. (a, b) Western blot for the levels of p-p38. (c, d) DHE assays of the levels of ROS in Raw 264.7 cells after treatmetns with various types of MSN@PEG at 200 μg mL^{-1} for 4 h and 24 h. (a, c) in serum-free media; (b, d) in serum-containing media.

Figure 3

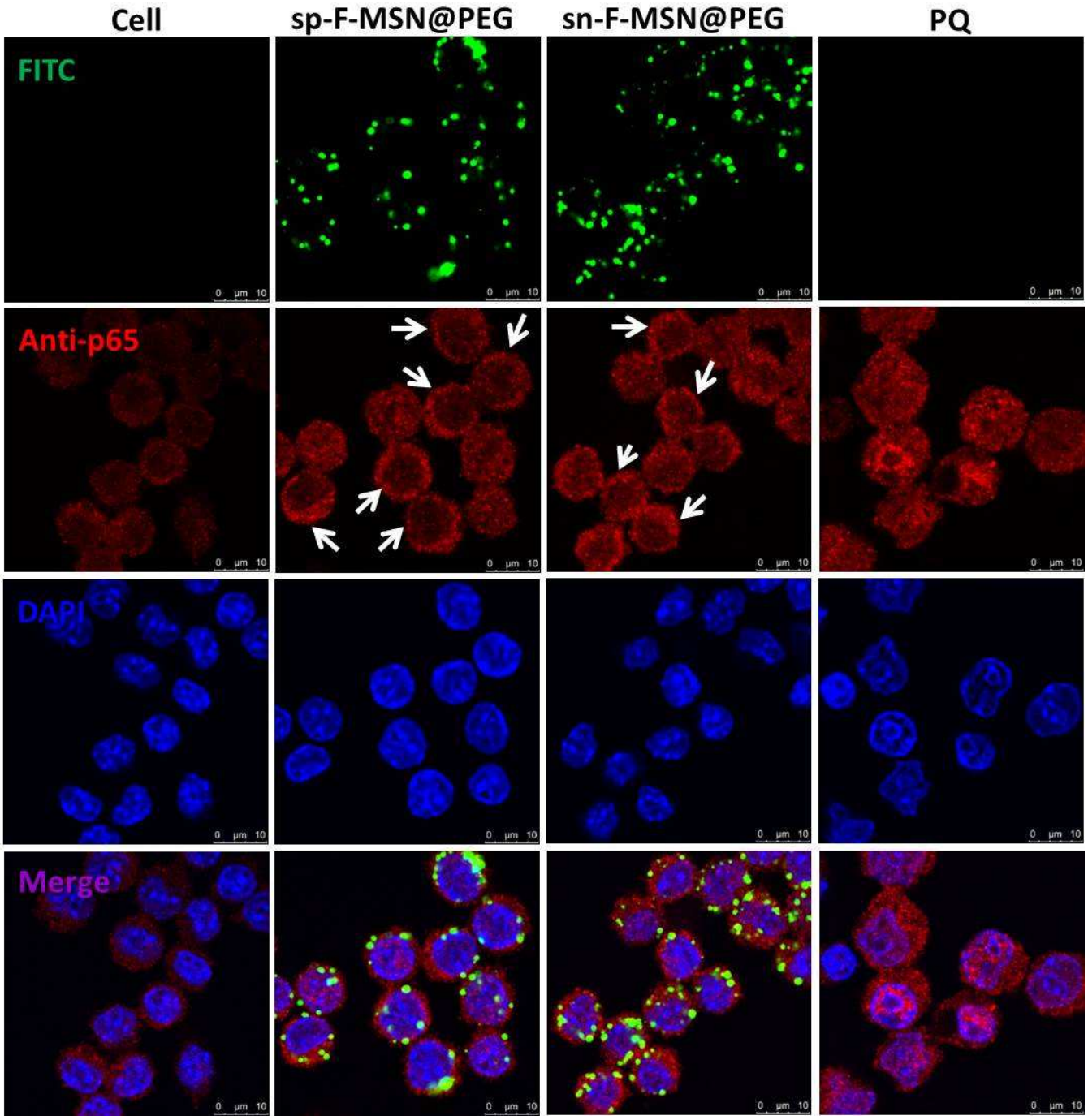

Figure 3. Confocal images of Raw 264.7 cells after treatmetns with nanoparticles at 200 μg mL^{-1} for 4 h in serum-containing media. Shown cell nucleus (DAPI-labeled, blue), nanoparticles (FITC-labeled, green) and p65 (Alexa-568-labeled anti-p65 antibody, red). The white arrows indicate cells with predominantly cytoplasmic distribution of NF-κB p65.

Figure 4

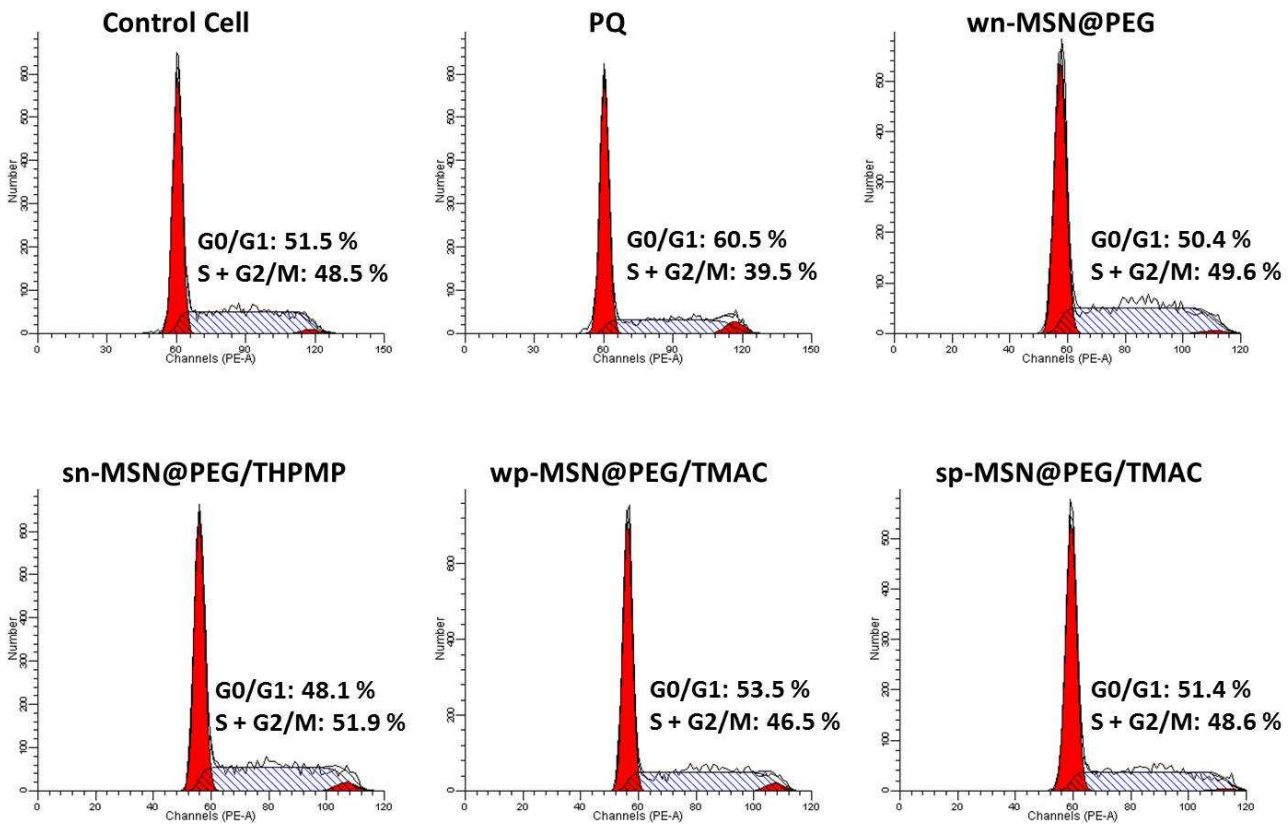

Figure 4. Cell cycle analyses of Raw 264.7 cells after treatmetns with various types of MSN@PEG for 4 h in serum-containing media. The graphs are representatives of the three independent experiments, each with similar results. The concentration of PQ and nanoparticles are 0.5 mM and 200 μg mL^{-1}, respectively.

Figure 5

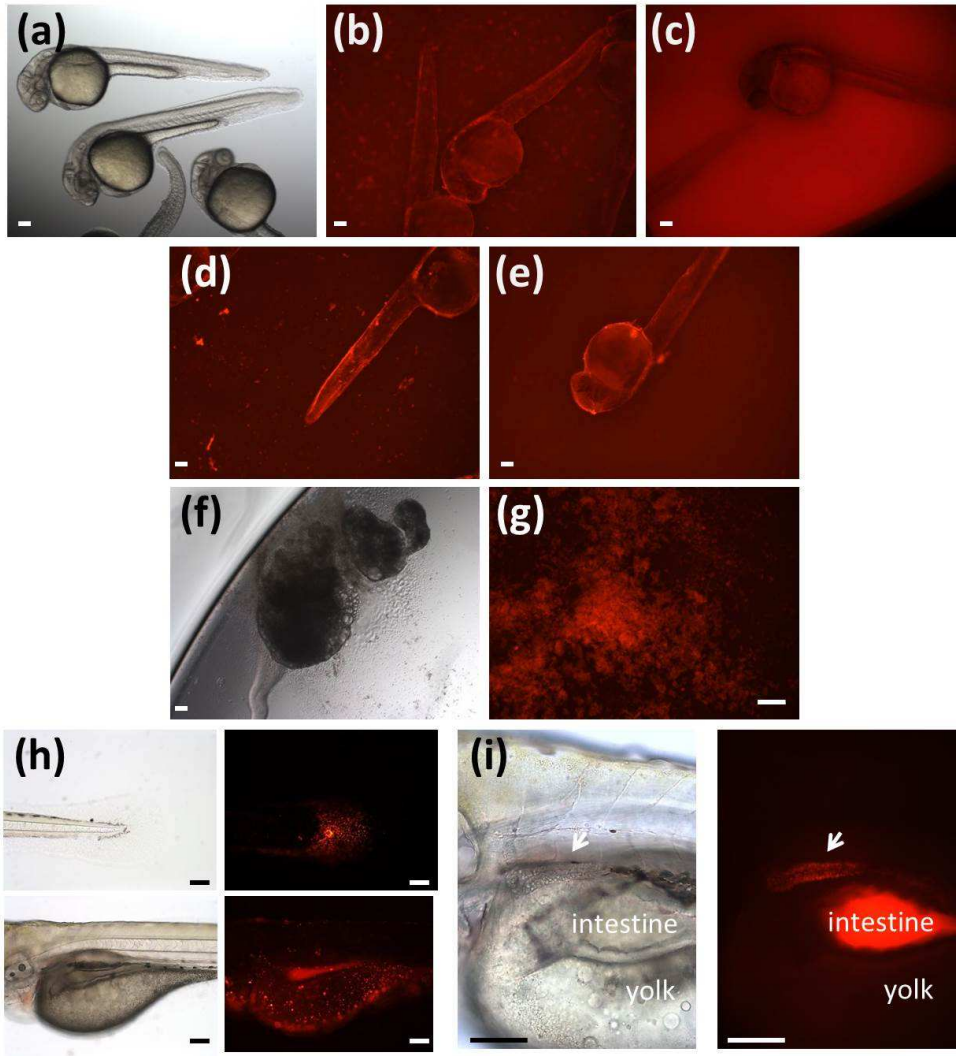

Figure 5. Optical images of embryonic zebrafish observed after exposure to nanoparticles for (a-f) 5 h, i.e. at 25 hpf stage; (g, h) 96 h, i.e. at 4 dpf stage. (a) Control; (b) 50 μg mL^{-1} of wn-R-MSN@PEG; (c) 50 μg mL^{-1} of sn-R-MSN@PEG/THPMP; (d) 50 μg mL^{-1} of wp-R-MSN@PEG/TMAC; (e) 50 μg mL^{-1} of sp-R-MSN@PEG/TMAC; (f,g) 100 μg mL-1 of sp-R-MSN@PEG/TMAC; (g) after sp-R-MSN@ PEG/TMAC treated epidermis disruption release embryo cells; (h) 100 μg mL^{-1} of wp-R-MSN@PEG/TMAC; (i) 100 μg mL^{-1} of sn-R-MSN@PEG/THPMP. The white arrows indicate protonephridium. Bar: 100μm.